Physical scale modeling the millimeter-wave backscattering behavior of ground clutter

A. J. Gatesman[*a], T. M. Goyette[a], J. C. Dickinson[a], J. Waldman[a], J. Neilson[b], and W. E. Nixon[b]

[a]Submillimeter-Wave Technology Laboratory, University of Massachusetts Lowell
Lowell, MA 01854

[b]U.S. Army National Ground Intelligence Center, 220 Seventh Street
Charlottesville, VA 22902

ABSTRACT

The VV-polarized W-band backscattering behavior of homogeneous ground clutter has been investigated by measuring the radar cross section per unit area of 1/16th scale rough surface terrain in a 1.56 THz compact radar range. An array of scale model ground planes was fabricated with the appropriate roughness to model smooth to rough soil terrain. In addition to studying the backscattering behavior as a function of surface roughness, the dependence on soil moisture content was also characterized by tailoring the dielectric constant of the scale models. Radar imagery of the rough surfaces were acquired in a 1.56 THz compact radar range by collecting single frequency backscatter data over a solid angle in both azimuth and elevation. The data were Fourier transformed in both the azimuth and elevation directions to produce two-dimensional imagery. The backscattering coefficient per unit illuminated area (σ^0) was calculated as a function of elevation angle between 5° and 85°. The results of this work have been used in the fabrication of scale model ground planes for collection of W-band radar imagery from scaled threat targets in realistic environments. Backscattering data, including clutter statistics, are compared to W-band clutter data found in the literature.

Keywords: W-band, terrain, clutter, backscattering, rough surfaces

1. INTRODUCTION

1.1. Overview

For the past twenty years, Expert Radar Signature Solutions (ERADS) under funding from the National Ground Intelligence Center (NGIC) has developed state-of-the-art scale model measurement systems to acquire radar signatures in support of a number of advanced radar applications such as automatic target recognition (ATR) systems, low-observable target evaluation, RAM development, and buried object detection. ERADS has developed fully polarimetric compact ranges at 160 GHz[1], 520 GHz[2], and recently, 1.56 THz[3] for acquisition of X-band, Ka-band, and W-band radar imagery of 1/16th and 1/48th scale model targets and scenes.

In order to acquire realistic signatures, the scaled target is usually placed on a ground plane modeling both the roughness and dielectric constant of common battlefield environments (sand, soil, grassy field, asphalt, concrete, etc.). The necessary dielectric scaling technology[4,5] has been developed to properly model non-metallic components of the targets as well as common ground terrain simulating different operational environments in which U.S. forces may be deployed. Proper modeling of the target/ground interaction is necessary if signature data collected from such compact ranges are to be exploited for automatic target recognition efforts, programming of smart munitions/weapons, testing of predictive codes, etc. To determine if realistic environments could be modeled properly in the newly developed 1.56 THz compact range (which models W-band at 1/16th scale), backscattering

[*] correspondence: email: andrew_gatesman@uml.edu; telephone: 978-458-3807; fax: 978-452-3333

Report Documentation Page

Form Approved
OMB No. 0704-0188

1. REPORT DATE	2. REPORT TYPE	3. DATES COVERED
SEP 2001		**00-00-2001 to 00-00-2001**

4. TITLE AND SUBTITLE	5a. CONTRACT NUMBER
Physical scale modeling the millimeter-wave backscattering behavior of ground clutter	5b. GRANT NUMBER
	5c. PROGRAM ELEMENT NUMBER
6. AUTHOR(S)	5d. PROJECT NUMBER
	5e. TASK NUMBER
	5f. WORK UNIT NUMBER
7. PERFORMING ORGANIZATION NAME(S) AND ADDRESS(ES) **University of Massachusetts Lowell,Submillimeter-Wave Technology Laboratory,175 Cabot Street,Lowell,MA,01854**	8. PERFORMING ORGANIZATION REPORT NUMBER
9. SPONSORING/MONITORING AGENCY NAME(S) AND ADDRESS(ES)	10. SPONSOR/MONITOR'S ACRONYM(S)
	11. SPONSOR/MONITOR'S REPORT NUMBER(S)

12. DISTRIBUTION/AVAILABILITY STATEMENT
Approved for public release; distribution unlimited

13. SUPPLEMENTARY NOTES
The original document contains color images.

14. ABSTRACT

15. SUBJECT TERMS

16. SECURITY CLASSIFICATION OF:			17. LIMITATION OF ABSTRACT	18. NUMBER OF PAGES	19a. NAME OF RESPONSIBLE PERSON
a. REPORT	b. ABSTRACT	c. THIS PAGE			
unclassified	**unclassified**	**unclassified**		**12**	

measurements were made on a variety of rough surfaces and compared with full-scale measurements at W-band. This paper examines the 1.56 THz backscatter response of 1/16th scale rough surfaces as a function of elevation angle, roughness, and dielectric constant to determine the potential of modeling realistic W-band behavior of ground terrain at scale model frequencies. In this paper, elevation angle is defined such that 90° elevation corresponds to normal incidence. The statistical behavior of the data was also examined by applying the Rayleigh fading model to the imagery as a function of reflectivity, roughness, and elevation angle.

1.2. Scale Modeling Dielectric Materials

Electromagnetic modeling the radar frequency behavior of materials at millimeter/submillimeter wavelengths requires that both the dielectric properties and dimensionality of the full-scale component be scaled properly. Scale modeling dielectric materials requires[6] that C_1 and C_2, which can be derived from Maxwell's equations as:

$$C_1 = \mu(\omega)\,\varepsilon'(\omega)(l\,f)^2, \text{ and } C_2 = \mu(\omega)\sigma(\omega)\,l^2 f \quad , \qquad \text{Eq. (1)}$$

are invariant to a change in scale.[7] In these equations, $\mu(\omega)$ is the material's permeability, $\varepsilon'(\omega)$ is the material's bound charge dielectric constant, l is a characteristic length on the full-scale target, and f is the full-scale radar frequency. Invariance may be achieved for C_1 by decreasing the characteristic length l and increasing the frequency f by the same scale factor while maintaining the same magnetic permeability and dielectric constant. Similarly, invariance of C_2 is achieved by increasing the material's conductivity $\sigma(\omega)$ by the same scale factor. Note that the relationships for C_1 and C_2 are independent, since $\varepsilon'(\omega)$ used in Eq. (1) takes only bound charges into account and not free carriers, such that $\varepsilon'(\omega)$ is independent of $\sigma(\omega)$. The dielectric constant $\varepsilon'(\omega)$ can still be complex and therefore describe absorption in the material. When scaling dielectric materials ($\sigma(\omega) = 0$), invariance in C_2 is trivial, i.e. $C_2 = 0$, and the only remaining requirement (in addition to scaling l and f) is that $\varepsilon'(\omega)$ and $\mu(\omega)$ of the scaled material be equal to that of the corresponding full-scale structure. These requirements are summarized as:

$$\mu(\omega)_{\text{scale model}} = \mu(\omega)_{\text{full scale}} , \qquad \text{Eq. (2)}$$

$$\varepsilon'(\omega)_{\text{scale model}} = \varepsilon'(\omega)_{\text{full scale}} . \qquad \text{Eq. (3)}$$

Typically, full-scale and scale model materials of interest are non-magnetic ($\mu = 1$) making Eq. (2) easily satisfied. Since the dielectric constant is typically frequency dependent, Eq. (3) requires that the scale model and full-scale material be different.

After the materials of the vehicle and terrain of interest have been identified, the radar dielectric properties are measured on an HP-8510 Network Analyzer using free-space, waveguide, or coaxial measurement techniques. When available, dielectric constants are taken from the literature. Meeting the requirement of Eq. (3) is accomplished by fabricating the scale model component from epoxy resins and silicone-based materials loaded with specific amounts of powdered agents (silicon, carbon, aluminum, copper, stainless steel, etc.) to achieve the full-scale dielectric constant at the scale model frequency. Figure 1 shows the real and imaginary parts of the dielectric constant of castable polyurethane plastic as a function of graphite powder loading.

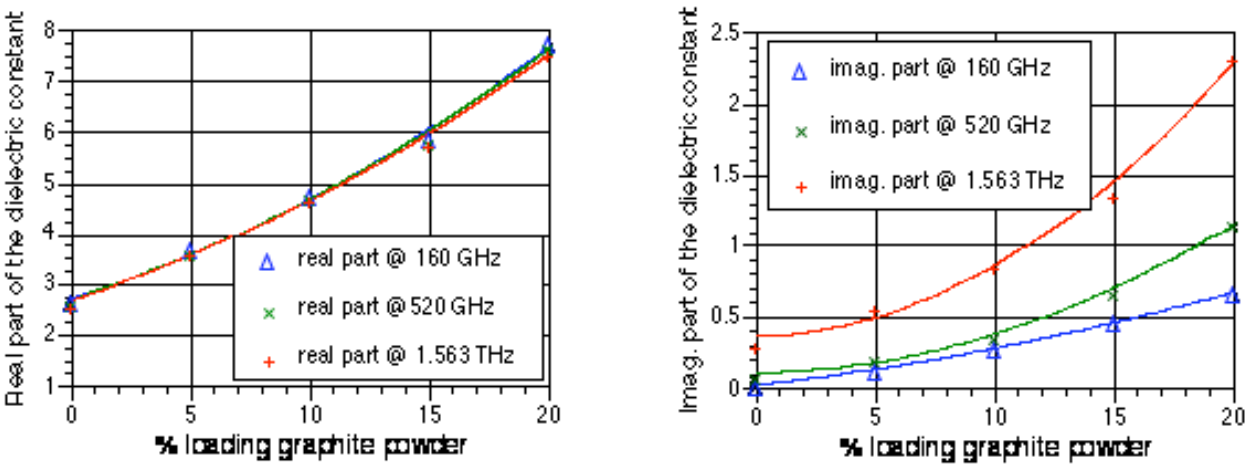

Figure 1. Real and imaginary parts of the dielectric constant for graphite-loaded polyurethane.

The data in Figure 1 demonstrate that the real part of the dielectric constant can be adjusted over a very wide range. The range of reflectivity of the graphite-loaded epoxy in Figure 1 is ≈ 5% - 25%. Most non-metallic materials of interest in the battlefield (tire rubber, fiberglass, plastics, composites, sand, soil, concrete, etc.) fall into this range. It is true that the real and imaginary components of the dielectric constant are not independently controlled, but by suitable choice of loading agent and host resin, virtually any material of interest can be adequately modeled. Some common radar materials and their scale model equivalents are given in Table I below.

Table I. Common Radar Materials and their Scale Model Equivalents

Category	Radar Material	Radar Frequency	Dielectric Constant	Radar Reflectivity	Scale Model Material	Scaled Frequency	Dielectric Constant	Scale Model Reflectivity
Terrain	Soil (little moisture)	10 GHz	3.4 + i 0.2	8.7%	loaded plastic	160 GHz	3.4 + i 0.1	8.8%
	Soil (moist)	10 GHz	7.3 + i 1.8	22.1%	loaded plastic	160 GHz	7.3 + i 0.65	21.3%
	Soil (little moisture)	35 GHz	3.1 + i 0.3	7.5%	loaded plastic	520 GHz	3.1 + I 0.22	7.7%
	Soil (moist)	35 GHz	4.9 + i 2.1	16.5%	loaded plastic	520 GHz	5.5 + i 0.6	16.3%
	Soil (little moisture)	94 GHz	2.9 + i 0.2	6.7%	loaded plastic	1.563 THz	2.9 + i 0.4	7.0%
	Soil (moist)	94 GHz	3.7 + i 1.2	11.3%	loaded plastic	1.563 THz	4.0 + i 0.6	11.4%
	Asphalt	10 GHz	4.3 + i 0.1	12.2%	loaded plastic	160 GHz	4.2 + i 0.13	11.9%
	Concrete	35 GHz	2.5 + i 0.65	5.8%	loaded plastic	520 GHz	2.59 + i 0.16	5.5%
Composites	E-glass/epoxy	10 GHz	4.5 + i 0.01	12.9%	Boron Nitride	520 GHz	4.84 + i0.004	14.1%
	E-glass/polyest.	10 GHz	4.1 + i 0.06	11.5%	Boron Nitride	520 GHz	4.84 + i0.004	14.1%
	Kevlar 49/polyest.	10 GHz	3.4 + i 0.07	8.8%	Polyimide	520 GHz	3.5 + i 0.07	9.2
Rubber	tank side skirt	10 GHz	2.5 + i 0.047	5.1%	plexiglass	160 GHz	2.59 + i 0.02	5.5%
	M-35 tire	10 GHz	6.9 + i 0.56	20.2%	loaded plastic	160 GHz	6.9 + i 0.53	20.2%
	SA-9 tire	35 GHz	7.7 + i 0.38	22.1%	loaded plastic	520 Ghz	7.6 + i 0.5	22.1%
Misc.	windshield glass	10 GHz	5.9 + i 0.15	17.3%	Schott AF-45	520 GHz	5.9 + i 0.33	17.4%
	Teflon	35 GHz	2.01 + i 0.0004	3.0%	Teflon	520 GHz	1.96 + i 0.003	2.8%

ERADS has used dielectric scaling and model building technology to establish a library of more than 100 high-fidelity 1/16th and 1/48th scale model tactical targets as well as rough and smooth ground terrain in support of radar signature measurement programs at 160 GHz, 520 GHz, and 1.56 THz. Figure 2 shows three of these models that have been used in various measurement programs. Representative structures included composite panels, radomes, frequency selective surfaces, tires, sideskirts, absorbers, etc.

- **Multi-layer composite panels (E-glass/epoxy, Kevlar, fiberglass)**
- **Frequency selective structures**
- **Rubber tires, track pads, side skirts**
- **Wood, glass, plastic structures**

Figure 2. Dielectrically scaled structures incorporated into a scale model Advanced Enclosed Mast Sensor/System (AEM/S) (left), a 1/16th scale HMMWV (center), and a 1/16th scale M1 tank (right).

1.3. Radar Modeling Rough Surfaces and Rayleigh Fading Statistics

When modeling highly complex geometry such as the surface of a rough dirt field, the statistical behavior of the scene is modeled instead of trying to match its exact geometry. The statistical quantity of interest is the backscattering coefficient σ^0 (unitless) defined as the radar cross section per unit area. For simplicity, only homogeneous scenes have been modeled meaning that the terrain exhibits the same local characteristics in terms of rms roughness, reflectivity, etc. for any location within the scene. In the radar imagery presented here, each resolution cell was sufficiently large such that several scatterers contributed to that cell's cross section. In addition, the number of resolution cells was sufficiently large so that the statistical properties of σ^0 could be examined over a given scene. The above features satisfy three assumptions required to apply Rayleigh fading statistics to the backscattering behavior of rough surfaces. The Rayleigh model was chosen because the surfaces studied are spatially homogenous. If the surfaces were heterogeneous, other distributions types, such as the K-distribution might be more appropriate. The model's assumptions are, 1) each resolution cell should contain several scatterers, 2) the scatterers are randomly distributed, and 3) the strengths of the scatterers are comparable in magnitude (i.e., no one (or a few) scatterers dominate over the others). Since the above assumptions are usually satisfied for many common types of terrain at radar frequencies, the Rayleigh model has been successful in describing the backscattering behavior of several types of statistically homogeneous terrain at W-band.[8,9]

According to the Rayleigh fading model, the scattered power per unit area on the ground for a particular scene is exponentially distributed. In other words, the backscattering coefficient for an individual resolution cell { EMBED Equation.3 } behaves like a random variable with an exponential probability density function (pdf) given by:

{ EMBED Equation.3 }

$$p(\sigma^o_{cell}) = \frac{1}{\sigma^o_{scene}} \exp[-(\sigma^o_{cell}/\sigma^o_{scene})] \qquad for\ \sigma^o_{cell} \geq 0,$$
$$p(\sigma^o_{cell}) = 0 \qquad for\ \sigma^o_{cell} < 0, \qquad \text{Eqs.(4)}$$

where { EMBED Equation.3 } is the average backscattering coefficient for the imaged area. As in Ref. 8, the "fading random variable" F was introduce as { EMBED Equation.3 }so the pdf reads:

$$p(F) = \exp[-F] \qquad for\ F \geq 0$$
$$p(F) = 0 \qquad for\ F < 0 \qquad \text{Eqs.(5)}$$

For the simple pdf given here, the mean value F_{ave} and the standard deviation s_F of the normalized random variable F are:

$$F_{ave} = s_F = 1.$$

The Rayleigh fading model was shown in Ref. 8 to be extremely good at predicting the backscattering statistics of several types of terrain at W-band at elevation angles ranging from 2° - 20°. The data collected here indicate that this statistical model works very well for 1/16th scale terrain at W-Band x 16 (1.56 THz) over a wide range of elevation angles.

2. FABRICATION OF SCALE MODEL ROUGH SURFACES

The 10-in.-diameter rough surfaces used in this study were prepared by casting dielectrically tailored plastics into molds with the appropriate rough surface. Full-scale soil terrain can have rms roughnesses which vary from ≈ 0.5 mm for surfaces smoothed out by a construction roller to ≈ 40 mm for a freshly plowed field.[8] The range of rms roughness studied here extended from 30 μm – 720 μm (or 0.5 mm – 12 mm full-scale) and therefore modeled only smooth to modestly rough surfaces. The ks values of the ground planes, where $k = 2\pi/\lambda$ and s = rms roughness, were 1.0, 4.9, 14.8, and 23.7. The reflectivities of the ground planes varied from 5% to 24% and well represented the entire range expected for dry to very moist (not quite saturated) soil at W-band (R≈6%-25%).[8] A total of 16 scale model ground planes were fabricated and are listed in Table II. Figure 3 shows ground plane 1B and close-ups of the four roughnesses used in this study.

Table II. Ground Plane Designation

reflectivity \ rms roughness	720 μm	450 μm	150 μm	30 μm
5%	1A	2A	3A	4A
10%	1B	2B	3B	4B
12%	1C	2C	3C	4C
24%	1D	2D	3D	4D

<- 10 inch diameter ground plane->

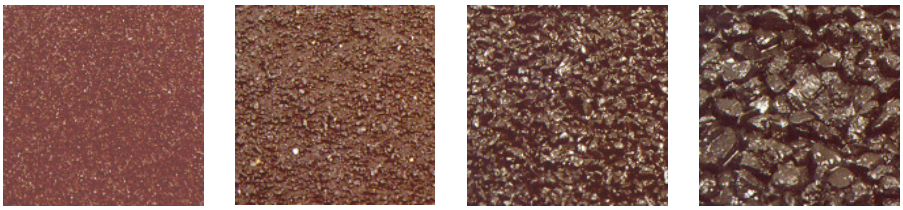

Figure 3. Roughnesses of the scale model ground planes. The images represent 1 sq. inch of each surface.

3. TWO-DIMENSIONAL AZIMUTH/ELEVATION IMAGERY AND ANALYSIS

3.1. Two-Dimensional Imaging Technique

Radar imagery of the 16 ground planes were measured in a 1.56 THz (λ = 0.192 mm) compact radar range specifically designed for acquisition of W-band imagery of 1/16th scale model tactical targets and scenes. A complete description of the system can be found in Ref. 3, so only a brief overview is given here. The coherent transceiver used two high-stability optically pumped far-infrared gas lasers, microwave/laser side-band generation for frequency agility, and a pair of Schottky diode receivers for coherent integration. The system was fully polarimetric, however, only VV data is reported in this work. The far-field system illuminates targets with a collimated, 18 in. two-way FWHM beam. The ground planes were 10-in.-diameter rough surface plates and therefore should have easily fit into the illuminating beam. However, due to the geometrical constraints of acquiring backscattering data over a very wide range of elevation angles, a portion of each elevation scan was collected with

the ground plane positioned in a shoulder region of the illuminating gaussian beam. To account for this effect on the data, a simple gaussian beam correction was applied to each image.

Though the radar system was developed to acquire conventional azimuth/range ISAR imagery, it was also capable of acquiring two-dimensional azimuth/elevation (Az/El) images. In this configuration, collecting single-frequency, coherent RCS data over a solid angle in azimuth and elevation directions allows an Az/El image to be formed using a two-dimensional Fourier transform. Because the frequency was fixed, no range information was recorded. However, such images are useful for creating a two-dimensional map of a target's scatterers as viewed from the radar's perspective (opposed to ISAR which provides a top-down view of the target) and also quite useful for analyzing the backscattering behavior of rough surfaces. Two-dimensional Az/El imagery was acquired for all 16 ground planes between 5° and 85° elevation. Figures 4 and 5 display VV-polarized Az/El imagery of ground planes 1B and 4B at 15°, 30°, 45°, 60°, and 75° elevation. Each pixel represents the radar cross section (in dBsm) for that given resolution cell. All imagery are plotted between a range of –60 dBsm and –20 dBsm. The axes of the imagery have been adjusted so that each image appears circular.

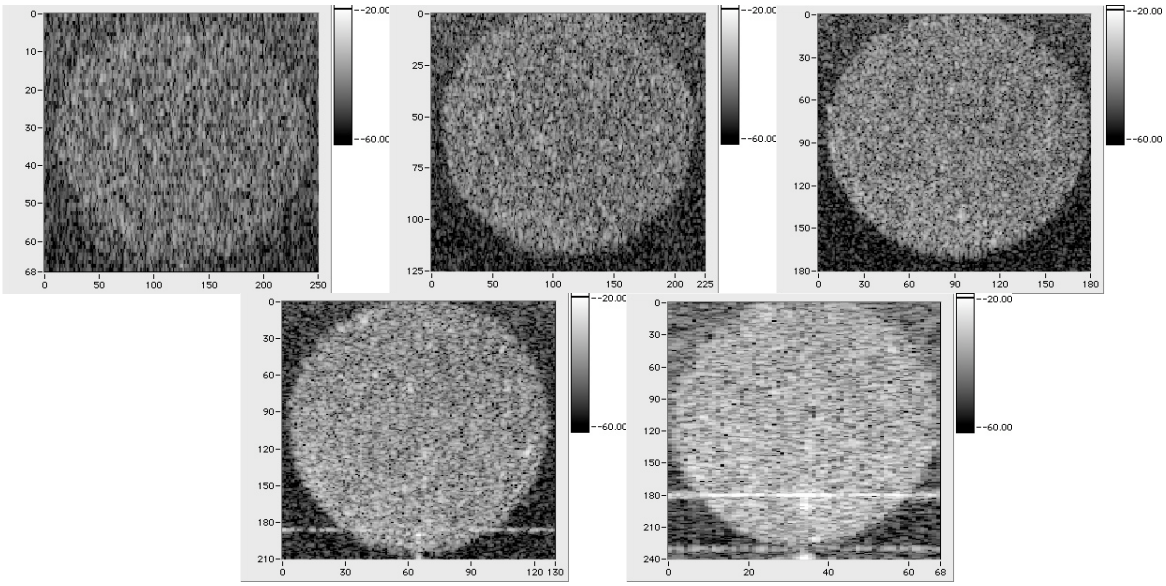

Figure 4. VV Az/El imagery of ground plane 1B at 15°, 30°, 45°, 60°, and 75° elevation.

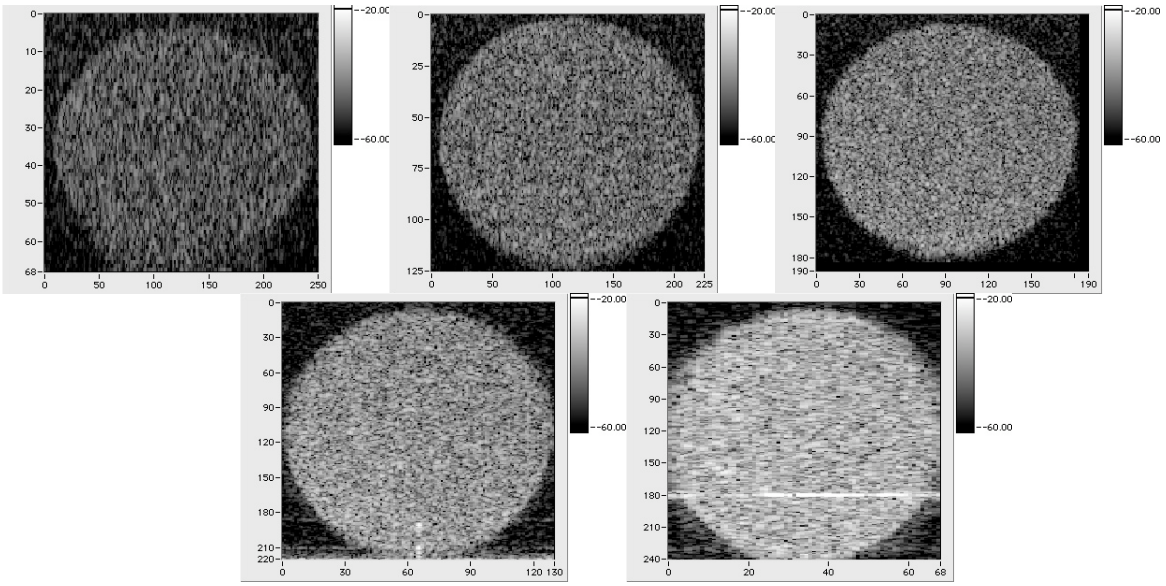

Figure 5. VV Az/El imagery of ground plane 4B at 15°, 30°, 45°, 60°, and 75° elevation.

To understand the resolution of the images, recall from standard ISAR processing[10] that cross-range resolution ΔX (whether azimuth or elevation) is determined by the total angular extent θ_t over which the data is coherently processed:

$$\Delta X \approx \frac{\lambda}{2\theta_t} \quad . \qquad \text{Eq. (6)}$$

The pixel area projected on the rough surface is then given by:

$$pixel \;\; area = \left(\frac{\lambda}{2\theta_t}\right)^2 \frac{1}{\sin(\theta_e)\cos(\theta_e)} . \qquad \text{Eq. (7)}$$

The $\sin(\theta_e)$ term takes into account that fact that the resolution cell was projected onto a surface at an elevation angle θ_e and the $\cos(\theta_e)$ term takes into account the reduction in azimuth resolution as the elevation angle increases. The data in Figures 4 and 5 were processed over angular windows of 5.12°, therefore, resolution cell areas varied from ≈4.5 mm^2 at elevation angles of 15° and 75° to ≈ 2.3 mm^2 at 45°.

3.2. General Behavior of Backscattering Coefficient σ^0

The general dependence of σ^0 on elevation angle can be divided into three regions:[11,12] low elevation angles, a plateau region, and high elevation angles. At low elevation, the surface will tend to appear smoother and σ^0 rapidly increases with increasing angle. At large angles, σ^0 also increases rapidly until it reaches a maximum at 90° (normal incidence). Between these two regions is a plateau region in which σ^0 is a weaker function of angle. The backscatter coefficient data for all 16 ground planes has been averaged and is shown in Figure 6. Overall behavior was similar to the expected general behavior of σ^0 with elevation angle. The backscattering coefficient rapidly increased with angle until approximately 20° where the increase slowed to ≈ 0.2 dB per degree. However, a rapid increase in σ^0 approaching normal incidence was not observed. The increase in σ^0 near 90° commonly cited in

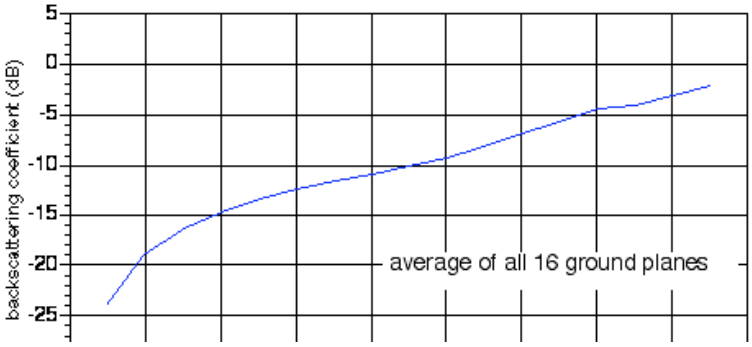

the literature is possibly due to the fact that the acceptance angle of a radar's receive optics is typically several degrees wide such that some of the forward scattered radiation is collected along with the backscattered radiation. A possible explanation for the lack of increase in σ^0 reported here is that the data were acquired in a true far-field configuration using a receiver with an extremely narrow acceptance angle (≈ 0.01°) such that even at 85°, no specular scattering was measured.

Figure 6. Average VV backscattering coefficient σ^0 vs. elevation angle for all 16 ground planes in Table II.

3.3. Dependence of σ^0 on Roughness and Reflectivity

The effect of surface roughness on the behavior of σ^0 was measured and is shown in Figure 7 for the 10% reflective ground planes. As listed in Table II, the actual rms roughnesses of the 1/16th scale ground planes were 30 μm, 150 μm, 450 μm, and 720 μm which correspond to full-scale rms values of 0.5 mm, 2.4 mm, 7 mm, and 12 mm. In Figure 7, differences in σ^0 were observed between 5° and 30° indicating that surface roughness had a greater impact on the lower elevation data.

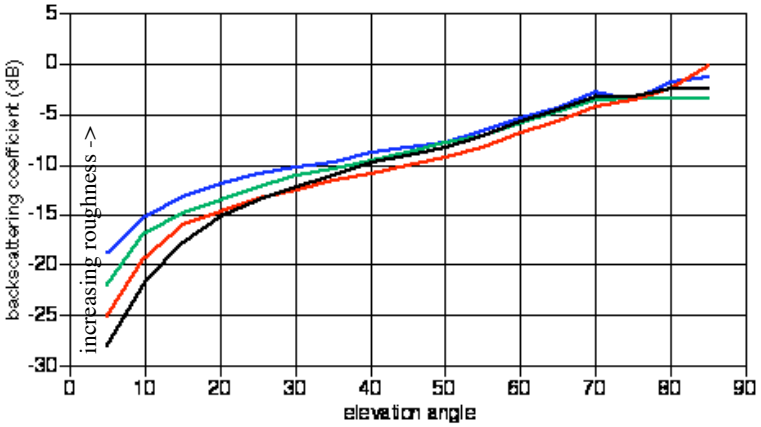

Figure 7. VV Backscattering coefficient vs. elevation angle for the four different roughnesses listed in Table II.

The dependence of σ^0 on reflectivity was also measured. Figure 8 shows σ^0 plotted as a function of elevation angle for ground planes with 5%, 12%, and 24% reflectivity. The ground planes had an rms roughness corresponding to 7 mm full-scale. A measurable increase in σ^0 with reflectivity was observed over all elevation angles. Note that the increase corresponds well with the increase in reflectivity. When the reflectivity increased from 5% to 24%, or by 6.8 dB, a similar increase in σ^0 was observed for nearly all elevation angles. This behavior was expected for surfaces rough compared with the wavelength. According to geometric optics,[13] σ^0 of a very rough surface is directly proportional to the surface reflectivity and largely independent of incident angle.

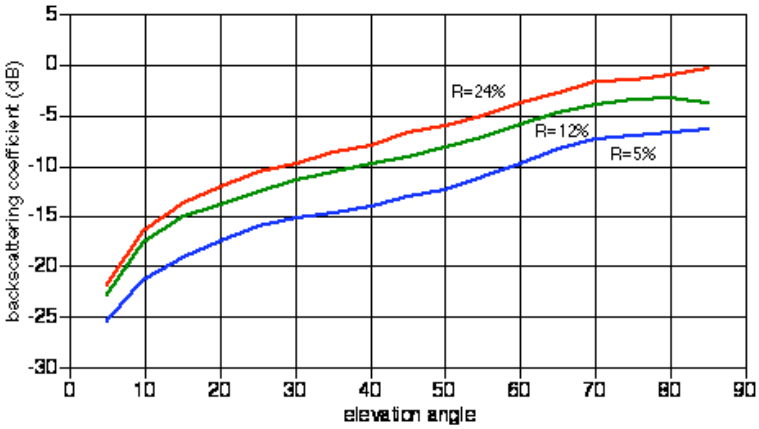

Figure 8. VV Backscattering coefficient vs. angle for three reflectivities of the 7 mm rms roughness (full-scale) ground plane.

3.4. Agreement of Scale Model Backscatter Data with Literature Values

Agreement of the scale model backscatter measurements with W-band data found in the literature was generally quite good. Figure 9 shows the upper (solid curve) and lower (dashed curve) limits of backscatter coefficient data compared with full-scale data acquired on a variety of terrain over a range of elevation angles. W-band backscattering data from Figure 4 and 9 of Ref. 8 have been overlaid for comparison. One of the data sets (Ref. 8, Figure 9) slightly exceeded our σ^0 data. However, this data set included several terrain types (including wooded terrain) in addition to bare soil surface and therefore was expected to be higher. Ref. 8, Figure 4 data from bare surfaces such as gravel, concrete, asphalt, and bare soil, fell well within the upper and lower limits of our measurements. Data from Ref. 14 that represents the W-band backscattering behavior for grass and crops was included for comparison as well.

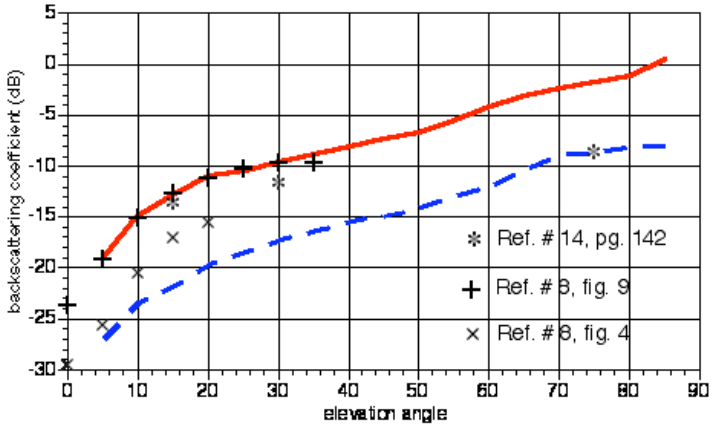

Figure 9. Upper and lower limits of σ^0 data compared with full-scale W-band data from Ref. 8 and 14.

3.5. Applying the Rayleigh Fading Model to Scale Model Clutter Imagery

When describing the fading (or scintillation) behavior of a distributed target such as ground terrain, it is common to model the return with one of the many distribution functions (Rayleigh, lognormal, Weibull, K–distribution, etc.) When the terrain being studied can be modeled as a large group of independent, randomly located scatterers, all of comparable strength, the Rayleigh distribution is usually most applicable. The fading statistics associated with this model have been highly successful in modeling fluctuating radar signals. The applicability of Rayleigh statistics to scale model W-band imagery of rough surfaces is demonstrate here. Statistics were generated for each of the 16 ground planes and the applicability of the model was tested as a function of elevation angle, roughness, and reflectivity. Statistics were generated by calculating F_i for each resolution cell by dividing a resolution cell's radar cross section { EMBED Equation.3 } by the average cross section of all cells in the scene { EMBED Equation.3 }. The Rayleigh fading model says that the probability F_i exists within a range ΔF is given by,

$$\text{probability} = p(F)\,\Delta F = e^{-F}\,\Delta F.$$

Fading statistics for the 12 mm and 0.5 mm rms roughness (full-scale) ground planes are shown in Figures 10 and 11. The quantity plotted is N $p(F)\,\Delta F$ where N is the number of pixels in the selected image. Therefore N $p(F)\,\Delta F$ represents the number of pixels with fading variables in the range ΔF for that particular value of F. As the plots indicate, the agreement with the Rayleigh model was extremely good. Though only the 10% reflective surfaces are shown here, no significant dependence on reflectivity was observed. Figures 10 and 11 represent the roughest and smoothest of the ground planes studied. Again, no significant dependence was observed over the range of roughnesses modeled here. Furthermore, an excellent fit to the model was observed as a function of elevation angle, even at the very high elevation angles.

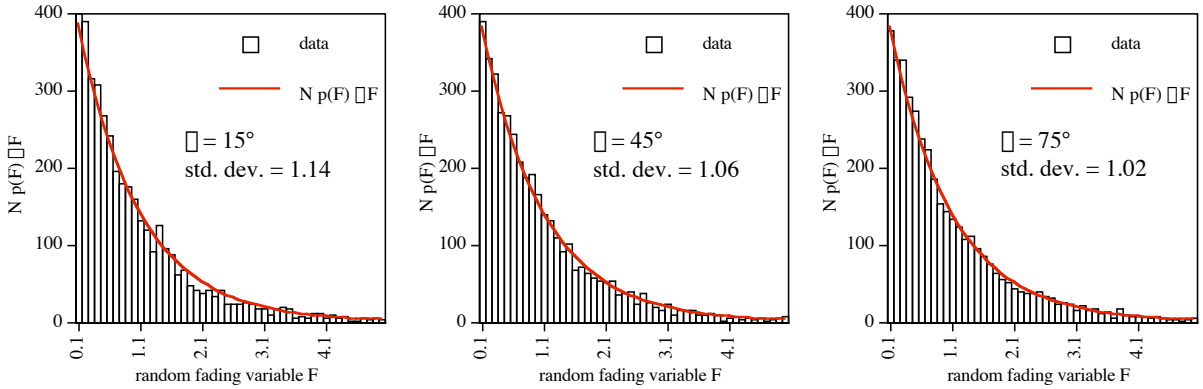

Figure 10. Comparison of measured data with the exponential prediction of the Rayleigh model for ground plane 1B (10% reflective, 12 mm rms roughness (full-scale)) at three different elevation angles.

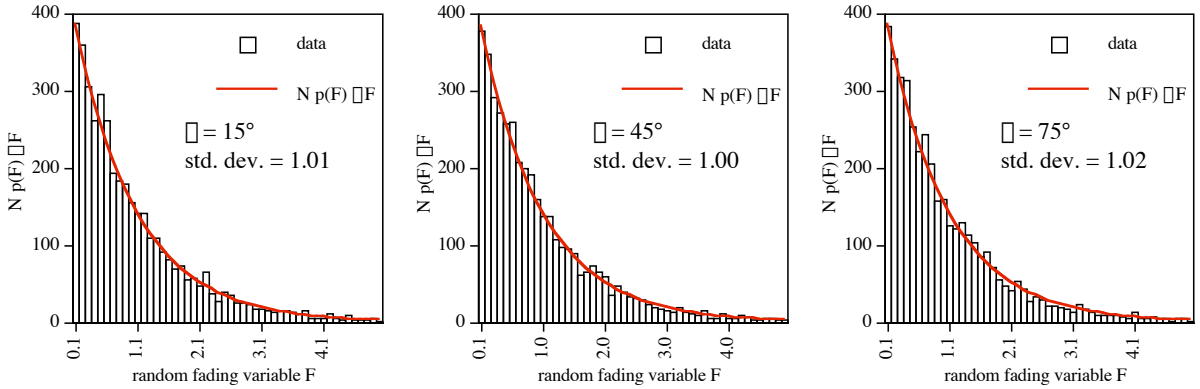

Figure 11. Comparison of measured data with the exponential prediction of the Rayleigh model for ground plane 4B (10% reflective, 0.5 mm rms roughness (full-scale)) at three different elevation angles.

The Rayleigh model states that the average value and standard deviation of F_i equal unity. The average value of F_i will always be one, however, the standard deviation s_F will vary depending on how well the imaged data fits the Rayleigh model. Table III lists the standard deviation of F_i for each of the 16 ground planes at three elevation angles (15°, 45°, 75°). Excellent agreement with the Rayleigh model was observed for virtually all ground planes at all elevation angles studied. Slightly better agreement was observed for the smoother ground planes. The data in Table III that corresponds to Figures 10 and 11 have been highlighted.

Table III

(Highlighted data are shown graphically in Figures 10 and 11)

Standard Devation of F(i)				
		elevation angle		
RMS roughness (full-scale)	Ft. surface reflectivity	15°	45°	75°
12 mm	5%	1.22	1.21	1.04
	10%	1.14	1.06	1.02
	12%	1.10	1.03	1.07
	24%	1.21	1.08	1.06
7 mm	5%	1.18	1.06	1.03
	10%	1.11	1.03	1.00
	12%	1.15	1.06	1.03
	24%	1.12	1.02	1.00
2.4 mm	5%	1.03	1.02	1.04
	10%	1.04	1.03	1.02
	12%	1.05	0.99	0.99
	24%	1.02	1.00	1.01
0.5 mm	5%	1.01	1.02	1.03
	10%	1.01	1.00	1.02
	12%	1.01	0.99	0.98
	24%	0.96	1.04	1.05

4. CONCLUSION

The backscattering characteristics of rough soil terrain at W-band have been investigated by acquiring two-dimensional Az/El radar imagery of 1/16th scale rough surfaces in a 1.56 THz compact radar range. Several ground planes were dielectrically and geometrically scaled to model soil surfaces with a variety of roughnesses and reflectivities. Radar imagery was analyzed and the dependence on surface roughness, reflectivity, and elevation angle was examined. Measurements are in very good agreement with W-band data found in the literature indicating that W-band backscatter behavior from homogeneous terrain can be accurately scale modeled at 1.56 THz. The statistical behavior of the backscattering coefficient was well described by Rayleigh fading statistics for all roughnesses and reflectivities studied as well as over elevation angles ranging from 5° to 85°.

ACKNOWLEDGEMENTS

The authors wish to thank Keith Gingras, Vicky Holmes, and William Kersey for their assistance. This work was supported by the National Ground Intelligence Center (NGIC) under contract #DAHC-90-96-C-0011.

REFERENCES

1. M. J. Coulombe, T. Horgan, J. Waldman, J. Neilson, S. Carter, and W. Nixon, "A 160 GHz Polarimetric Compact Range for Scale Model RCS Measurements," Antenna Measurements and Techniques Association (AMTA) Proceedings, Seattle, WA, October 1996.

2. M. J. Coulombe, T. Horgan, J. Waldman, G. Scatkowski, and W. Nixon, "A 520 GHz Polarimetric Compact Range for Scale Model RCS Measurements," Antenna Measurements and Techniques Association (AMTA) Proceedings, Monterey, October 1999.

3. T. M. Goyette, J. C. Dickinson, J. Waldman, W. E. Nixon, and S. Carter, "Fully Polarimetric W-band ISAR Imagery of Scale-Model Tactical Targets Using a 1.56 THz Compact Range," Proceeding of SPIE 15th Annual Inter. Symp. on Aerospace/Defense, Simulation, and Controls, Vol. 4382, Orlando, FL, April 2001.

4. R. H. Giles, A. J. Gatesman, J. Fitz-Gerald, S. Fisk, and J. Waldman, "Tailoring Artificial Dielectric Materials at Terahertz Frequencies," The Fourth International Symposium on Space Terahertz Technology, April 1993, Los Angeles, CA.

5. R. H. Giles, A. J. Gatesman, A. P. Ferdinand, and J. Waldman, "Design and Fabrication of Narrow Band Radar Absorbing Materials at Terahertz Frequencies," IEEE Proceedings from the 15th International Conference on Infrared and Millimeter Waves, Orlando, FL, Dec. 1990.

6. G. Sinclair, "Theory of Models of Electromagnetic Systems," Proc. Inst. Radio Eng., Vol. 36 pp. 1364-1370, 1948.

7. J. A. Stratton, *Electromagnetic Theory*, Mc-Graw-Hill Book Company, New York, 1941.

8. F. T. Ulaby, A. Nashashibi, A. El-Rouby, E. S. Li, R. D. De Roo, K. Sarabandi, R. J. Wellman, and H. B. Wallace, "95-GHz Scattering by Terrain at Near-Grazing Incidence," IEEE Trans. on Antennas and Propagation, Vol. 46, No. 1, Jan. 1998.

9. F. T. Ulaby, T. F. Haddock, and R. T. Austin, "Fluctuation Statistics for Millimeter-Wave Scattering From Distributed Targets," IEEE Transactions of Geoscience and Remote Sensing, Vol. 26, No. 3, May 1988.

10. D. L. Mensa, *High Resolution Radar Cross-Section Imaging*, Artech House, Inc. Norwood, MA 1991.

11. M. W. Long, *Radar Reflectivity of Land and Sea,* D. C. Heath and Company, 1975.

12. N. C. Currie, and C. E. Brown, *Principles and Applications of Millimeter-Wave Radar*, Artech House, Inc. Norwood, MA 1987.

13. F. T. Ulaby, R. K. Moore, and A. K. Fung, *Microwave Remote Sensing*, Norwood, MA, Artech, 1982, vol. II, ch. 12.

14. N. C. Currie, R. D. Hayes, R. N. Trebits, *Millimeter-Wave Rader Clutter*, Norwood, MA, Artech, 1992.